Life-Cycle of Structures and Infrastructure Systems – Biondini & Frangopol (Eds)

Seismic fragility analysis of nonuniformly corroded irregular RC bridges

Ebrahim Afsar Dizaj
Department of Civil Engineering, Azarbaijan Shahid Madani University, Tabriz, Iran

Mohammad Reza Salami
School of Engineering and the Built Environment, Birmingham City University, UK

Mohammad Mehdi Kashani
Faculty of Engineering and Physical Sciences, University of Southampton, Southampton, UK

ABSTRACT: Reinforced Concrete (RC) bridges in over crossings are typically constructed with unequal-height piers. The resulting substructure irregularity triggers an unbalanced seismic behaviour of these bridges, which increases their seismic vulnerability. The seismic irregularity of such bridge structures might be further intensified if the piers of varying heights expose to unsymmetrical chloride-induced corrosion damage. To accurately evaluate the seismic vulnerability of corroded irregular RC bridges, this paper studies the seismic fragility of a benchmark multi-span irregular RC bridge with five different corrosion damage scenarios, including unsymmetrical corrosion of piers. Toward this objective, first, monotonic nonlinear pushover analysis is used to quantify the time-dependent seismic capacity limit states by employing an advanced three-dimensional nonlinear finite element model. Then, Incremental Dynamic Analysis (IDA) and seismic fragility analysis are carried out to investigate the nonlinear dynamic behaviour and vulnerability of selected corroded bridges. The results show that, depending on the corrosion scenario, the distribution of seismic ductility demands can be varied in unequal-height bents, which can change the critical bent within a bridge system. Furthermore, results indicate that severe unsymmetrical corrosion damage can cause a synchronised failure of unequal-height piers.

1 INTRODUCTION

Bridges supported on piers of unequal heights are commonly the only construction choice in over-crossings (Kappos et al. 2002, Guirguis and Mehanny 2012). The substructure irregularity of such bridges triggers unbalanced distribution of seismic ductility demand among the piers of varying heights. Some design codes provide recommendations to ensure the regular seismic behaviour of multi-span RC bridges (AASHTO 2011, Caltrans 2013). Moreover, several methodologies have been proposed in the literature to mitigate the unbalanced distribution of seismic demand in irregular multi-span RC bridges (Priestley 2007, Xiang and Li 2020, Ishak and Mehanny 2017, Jara et al. 2013).

The seismic behaviour analysis of irregular RC bridges has been widely studied in the literature (Soleimani et al. 2017, Soltanieh et al. 2019, Hu & Guo 2020, Saiidi et al. 2012, Camacho et al. 2022). Gomez-Soberon et al. (2019) evaluated the seismic behaviour of highway bridges with different irregularity conditions. Their results showed that the adjacent piers of unequal heights considerably affect the vulnerability of concrete bridges. Sensitivity analyses on RC bridges with various irregularity conditions conducted by Soleimani et al. (2017) indicated

DOI: 10.1201/9781003323020-411

that earthquake intensity level, pier height, pier diameter, longitudinal reinforcement ratio, concrete compressive strength, and span length are the most important parameters determining the seismic performance of RC bridges with the irregular layout. Hu and Guo (2020) evaluated the seismic response of high-speed railway bridge-track systems with unequal-height pier configurations. The results showed that increasing the height difference of adjacent bridge piers intensifies the seismic displacement responses of the shear alveolar, moveable bearings, and sliding layer. Jara et al. (2015) found that hard soil ground motion records cause moderate damage in bridge columns, whereas soft soil records trigger considerable damage in columns.

Over the past few years, corrosion damage and ageing of RC bridges have become a challenging problem among structural engineers and bridge owners (ASCE 2021, Ghosh & Sood 2016, Afsar Dizaj& Kashani 2022, Afsar Dizaj et al. 2021). A survey conducted by Department for Transport and Highways England estimated that corrosion damage to concrete bridges costs about £1 billion/per year in England and Wales (Comptroller and Auditor General 2014, Broomfield 2007). Pevious studies on seismic fragility assessment of corroded concrete bridges commonly supposed a uniform corrosion scenario, where the average time-dependent corrosion level of piers is assumed to be the same (Choe et al., 2009, Zhang et al. 2019). However, constructing bridges over highways, rivers, railways, and valleys leads to various corrosion scenarios in bridge piers. Therefore, the seismic behaviour of concrete bridges with substructure irregularity can be significantly affected if they are located in chloride-laden environments.

The nonuniform chloride-induced corrosion of piers can exacerbate the unbalanced seismic demand and affect the transverse seismic behaviour of irregular bridges. Moreover, it can change the pattern of demand distribution, affect the damage mechanisms, and alter the failure sequence of bents of varying heights. This paper aims to investigate the seismic performance and fragility of irregular nonuniformly corroded bridges.

2 BRIDGE DETAILS AND NUMERICAL MODELLING

2.1 *Geometry and details*

In this study, the details of a two-span RC bridge tested in the shake table facility of the University of Nevada are considered here to study the combined effects of corrosion damage and substructure irregularity on the seismic fragility of RC bridges (Johnson et al. 2008). Figure 1 shows the geometry and structural details of this prototype irregular benchmark RC bridge. As shown in Figure 2, the total bridge length is 2050.0 cm, and the span length is 914.0 cm; the clear height of the piers from the top of the foundation is 182.9 cm, 243.8 cm and 152.4 cm for bent 1, bent 2 and bent 3, respectively. Six 9.1 tons, two 10.8 tons, and two 2.3 tons of super-imposed weights are placed on the superstructure. Moreover, the diameter of all columns is 30.5 cm; the longitudinal reinforcement ratio is approximately ρ_l = 1.56%, and the spiral reinforcement ratio is ρ_s = 0.9%. Further details on the structural details and material properties of this bridge specimen can be found in (Johnson et al. 2008).

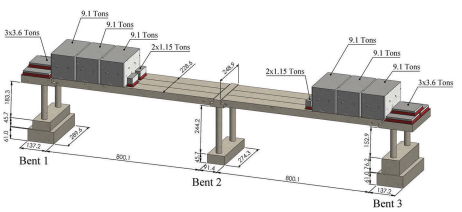

Figure 1. Geometry of the benchmark bridge.

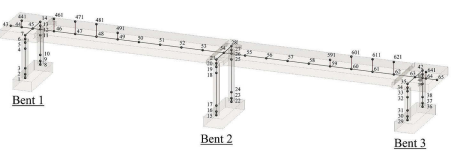

Figure 2. Three-dimensional finite element model of benchmark RC bridge.

2.2 *Finite element model*

In this study, the advanced nonlinear finite element modelling technique developed by Afsar Dizaj and Kashani (2022) is extended to simulate the nonlinear structural response of the benchmark RC bridge. The adequacy of this model in simulating seismic response of bridge piers under biaxial loading was demonstrated by Salami et al. (2019). Figure 2 shows the three-dimensional numerical model of the considered reference RC bridge. This model can simulate the inelastic buckling behaviour and low-cycle fatigue degradation of reinforcements. As Figure 2 shows, bridge piers and deck beams are divided into several fibre sections in their entire length in this model. Moreover, each component is modelled using five force-based elements: two zero-length section elements at the top and bottom to simulate the slippage of reinforcement at connection adjacents, two force-based elements with three integration points at the top and bottom and an intermediate element with five integration points. Further details about the developed model and numerical validation are available in Afsar Dizaj et al. (2022, 2023).

2.3 *Corrosion damage scenarios*

To investigate the influence of corrosion damage on the seismic fragility of the benchmark irregular concrete bridge, three corrosion statuses of piers, including (*i*) pristine, (*ii*) slightly corroded and (*iii*) highly corroded conditions, are considered. The material and geometrical properties of the corroded hypothetical bridge piers are updated using the mass loss ratio of rebars (ψ) in any of the corrosion statuses mentioned above. This parameter can be calculated using Equation 1 (Afsar Dizaj 2022):

$$\psi(t) = \left(\frac{d_b d_c - 1.05(1 - W/C)^{-1.64} t^{0.71}}{d_b d_c} \right)^2 \tag{1}$$

where d_c is cover thickness, d_b is the diameter of main bars; W/C is the water-to-cement ratio, and t is the time from corrosion initiation.

In this study, five different corrosion scenarios are considered. Scenario 1 is the benchmark bridge specimen tested by Johnson et al. (2008) where all the piers are considered pristine (uncorroded). In scenario 2, all the piers are assumed to be slightly uniformly corroded. For this scenario, it is assumed t=5 years; therefore, from Eq. (5), the mass loss ratio of spiral and longitudinal reinforcement is obtained as 15.8% and 5.5%, respectively. For scenario 3, it is assumed t=5 years; therefore, for this condition, the mass loss ratio of spiral and longitudinal reinforcement is calculated to be 50% and 18.9%, respectively. Therefore, in this scenario, all piers are severely corroded uniformly.

In addition to the uniform corrosion damage scenarios (scenarios 2 and 3), two nonuniform corrosion statuses are considered where the corrosion levels of different piers are assumed to be spatially variable. To this end, in scenario 4, the piers of bent 2 are taken to be severely corroded, and the others are slightly corroded. Finally, in scenario 5, while the piers of bent 1 and bent 2 are slightly corroded, the piers of bent 3 are assumed to be severely corroded.

3 CAPACITY LIMIT STATES

Nonlinear pushover analysis is carried out on the three bents of hypothetical bridge layouts with different corrosion levels to quantify the time-dependent capacity limit states. To this end, the material and geometrical properties of the frame are modified to incorporate corrosion-induced degradation. Moreover, the bases of the columns are assumed to be fully fixed, and the P-delta effects are also included in the analyses.

Figure 3 compares the capacity curves of bents with different corrosion percentages. The capacity limit states associated with bar yielding, cover concrete spalling, and core concrete crushing are mapped on each curve. Moreover, the onset of core concrete crushing is considered the onset of the collapse as it takes place just before a significant drop in capacity curves. As Figure 3 shows, the ductility and capacity of each bent significantly decrease as the corrosion level increases. Remarkably, the severely corroded bents experience a sudden drop in their post-peak response, showing a considerable decrease in their ductility. The capacity limit states quantified in this section are used in Section 4.3 to develop seismic fragility curves.

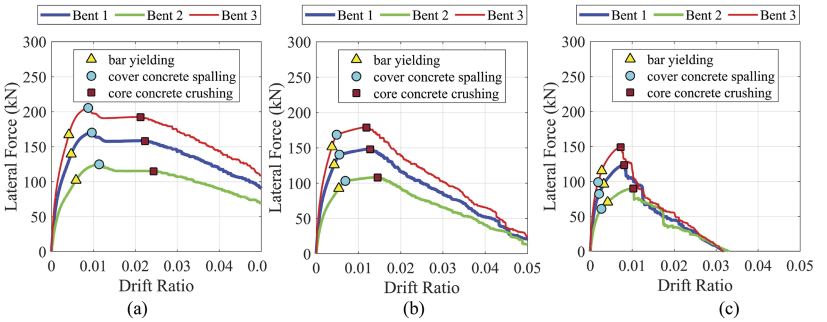

Figure 3. Capacity curves and capacity limit states: (a) uncorroded bents; (b) slightly corroded bents, and (c) severely corroded bents.

4 INCREMENTAL DYNAMIC ANALYSIS (IDA)

4.1 *Selected ground motions*

To carry out incremental dynamic analyses, 32 individual earthquake records are selected from the far-field ground motion records available in FEMA P695 (2009). Detailed information on the characteristics of selected ground motion records is provided in Afsar Dizaj et al. (2022, 2023). It should be noted that the primary transverse vibration mode of the reference bridge specimen is its second mode; therefore, selected ground motion records were scaled up by 0.1g steps (from 0 to 2.2g) in terms of $Sa(T_2,5\%)$ and used as input for incremental dynamic analyses.

4.2 *IDA results*

Figure 4 compares the median IDA curves of each bent to investigate the nonlinear behaviour and failure mechanism of the hypothetical bridge layouts. Figure 4 shows that median IDA response of all bents becomes a plateau at approximately $Sa(T_2, 5\%)$=1.2g. However, results show that for a given $Sa(T_2, 5\%)$, bent 1 experiences higher drift ratios. For example, while $Sa(T_2, 5\%)$=1g corresponds to approximately 0.039 peak drift ratio in piers of bent 1, for the same median intensity measure of ground motion records, bent 2 and bent 3 tolerate about 0.019 and 0.022 maximum drift ratios, respectively. This shows that 1 in scenario 1, bent 1 is more vulnerable than the other two bents. However, as Figure 4(c) shows, the median IDA response of all bents in the severely uniformly corroded bridge (i.e., scenario 3) is approximately identical. This can be due to the insufficient confinement in the piers of this bridge specimen as a result of the premature fracture of severely corroded spirals.

Figure 4(b) indicates that the slight uniform corrosion of piers causes a 25% reduction in the associated intensity level with the plateau response of bents. However, like the uncorroded bridge (scenario 1), bent 1 sustains higher displacement demands. This infers that the failure sequence of bents has not experienced a significant change compared to scenario 1. Figure 4(c)

show that the considerable reduction in the capacity of bents due to the severe uniform corrosion of piers results in near-synchronised flexural failure of all piers. Therefore, it can be inferred from the results presented in Figure 4(c) that all the bents fail almost simultaneously for the RC bridge supported on severely uniformly corroded piers. This can be attributed to the premature fracture of extremely corroded spirals, where the core concrete is almost unconfined.

Figure 4(d) shows that the onset of failure of columns of bent 2 (taller columns) coincides with that of columns of bent 3 (shorter columns). This implies that the higher ductility demand attracted by the stiffer piers of bent 3, is regulated significantly by the greater corrosion percentage of bent 2. Consequently, the columns of these two bents with different stiffnesses are collapsed at approximately the same intensity of input ground motions. Finally, Figure 5(e) shows that the nonuniform corrosion of piers in scenario 5 has resulted in the near-synchronised collapse of bent 1 and bent 3 at approximately Sa(T_2, 5%)=0.6g.

4.3 *Seismic fragility curves*

In this section, the failure probability of studied RC bridges is investigated. To this end, the following fragility function is used:

$$P[MDR \geq CLS \mid IM = y] = 1 - \Phi\left(\frac{\ln(\mathrm{CLS}) - \ln(\mu)}{\beta}\right) \tag{2}$$

where P[.] is the probability that the maximum drift ratio (MDR) exceeds a capacity limit state (CLS), given that the intensity measure (IM) equals y. Moreover, Φ(.) is the lognormal distribution function with the logarithmic mean, and standard deviation of ln(μ) and β, respectively, which can be obtained using Equations 3-4:

$$\ln(\mu) = \frac{\sum_{i=1}^{n} \ln(\mathrm{MDR}_i)}{n} \tag{3}$$

$$\beta = \sqrt{\frac{\sum_{i=1}^{n} (\ln(\mathrm{MDR_i}) - \ln(\mu))^2}{n-1}} \tag{4}$$

In Equations (3-4), n is the number of records, and $\mathrm{MDR_i}$ is the maximum drift ratio associated with a given value of IM for the i_{th} record. It is noteworthy that the MDR associated with concrete crushing (as shown in Figure 5) of piers is assumed as the collapse capacity limit state in Equation. (2).

Figure 5(a) shows that in scenario 1, the probability of failure of bent 1 is higher than in other bents. For instance, for IM=1.2g, while the failure probability of bent 1 is approximately 94%, it is around 62% and 71% for bent 2 and bent 3, respectively. Likewise, in Figure 5(b), the same trend can be seen with a slightly higher probability of collapse due to the uniform corrosion of piers. However, Figure 5(c) indicates that in scenario 3, the fragility curves of bent 2 and bent 3 are almost in line with that of bent 1. Especially for higher IMs (i.e., higher than IM=0.6g), the probability of collapse of all bents is approximately the same. This implies the near-synchronised brittle failure of bents, which is consistent with the conclusion of the IDA results presented in Figure 4(c).

Figure 5(d) compares the failure probability of bents in the nonuniformly corroded bridge scenario 4. As this figure shows, due to the higher degree of corrosion in the intermediate piers, the fragility curves of bent 3 and bent 2 are similar. This implies the synchronised failure of these two bents just after the failure of bent 1. Finally, Figure 5(e) shows that the fragility curve of bent 3 is on top of others.

This indicates that, in this scenario, the collapse probability of shorter columns is higher than others. Therefore, it can be concluded that various corrosion scenarios can result in diverse seismic behaviour and failure sequences of multi-span RC bridges with unequal-heigth piers.

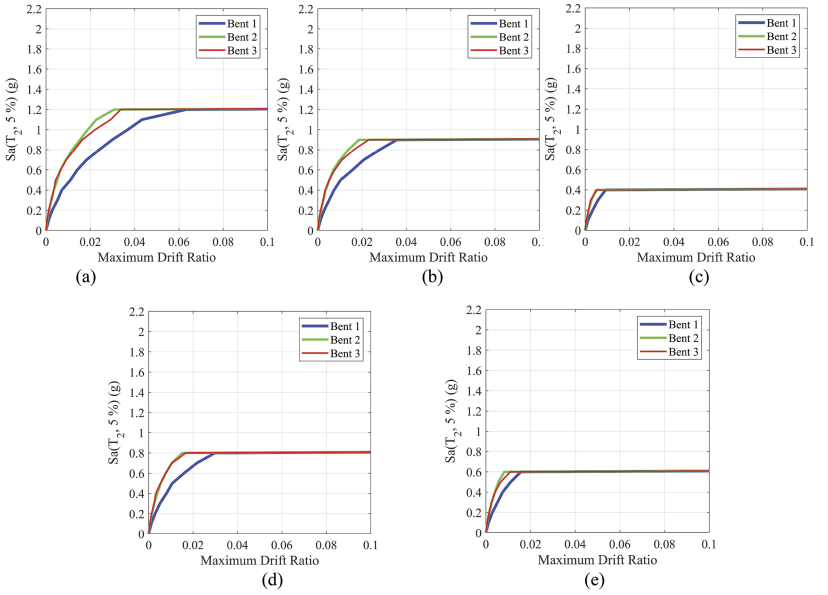

Figure 4. Median incremental dynamic analysis results: (a) scenario 1; (b) scenario 2; (c) scenario 3; (d) scenario 4, and; (e) scenario 5.

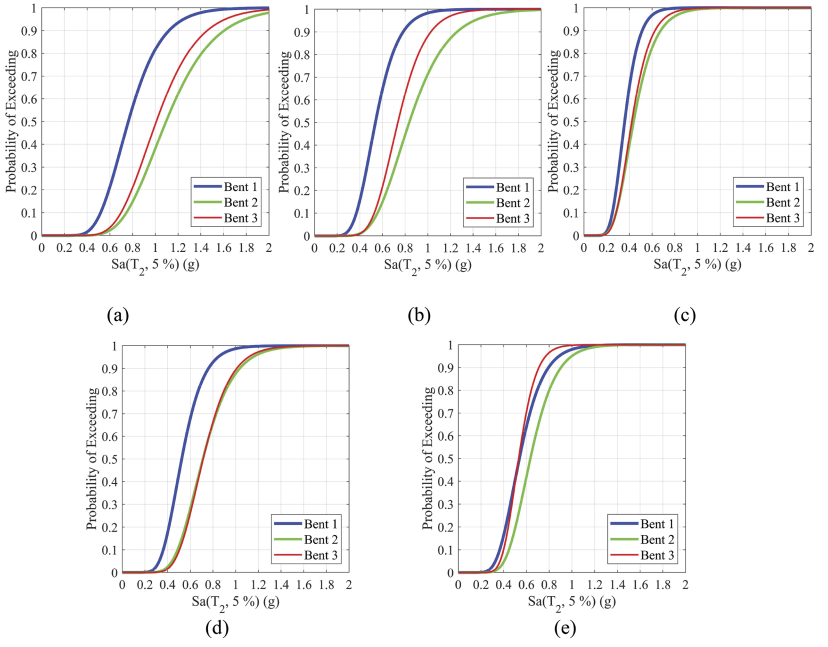

Figure 5. Collapse fragility curves of bents: (a) scenario 1; (b) scenario 2; (c) scenario 3; (d) scenario 4, and; (e) scenario 5.

5 CONCLUSIONS

This study evaluated the seismic performance and vulnerability of corrosion-damaged multi-span RC bridges with substructure irregularity. To this end, an advanced three-dimensional modelling methodology was employed to simulate the nonlinear behaviour of multi-span

irregular RC bridges accurately.The developed numerical model was then successfully verified against the large-scale shake table test results of an irregular two-span concrete bridge. Five hypothetical corrosion damage scenarios were considered, including uniform and nonuniform corrosion scenarios of piers. The failure modes and nonlinear dynamic behaviour of studied bridges with varied corrosion scenarios were assessed using nonlinear pushover and incremental dynamic analyses. Finally, the time-dependent fragility curves were developed using the IDA outputs for the frames under the selected ground motion suite.

The obtained results indicated that the unbalanced seismic demand distribution due to the substructure irregularity of the uncorroded bridge (scenario 1) causes the earlier failure of medium-height piers. This causes the higher vulnerability of bent 1 in this bridge specimen. The slight symmetrical corrosion level (around 5.5% in terms of rebar mass loss, t=5 years) of the bridge columns (Scenario 2) causes an approximately 25%, 35%, and 20% reduction in median failure IM of bent 1, bent 2, and bent 3, respectively. However, it does not affect the failure sequence of bents, where bent 1 tolerates higher seismic ductility demands than other bents. Moreover, results showed that the severe uniform corrosion of bridge piers (scenario 3) results in near-synchronised flexural failure of bents. This can be attributed to insufficient confinement in severely corroded bridge piers, resulting in brittle failure.The other important finding of the current study was that, depending on the corrosion damage scenario of piers, the nonuniform corrosion of bridge piers in an irregular RC bridge could regulate or exacerbate the unbalanced seismic ductility demand distribution across piers of unequal heights. For example, results showed that, in scenario 4, the adjusted seismic demand on severely corroded bent 2 results in the near-simultaneous collapse of taller and shorter piers.

REFERENCES

AASHTO. 2011. AASHTO Guide Specifications for LRFD Seismic Bridge Design. Washington: American Association of State Highway and Transportation Officials.

Afsar Dizaj, E. 2022. Modelling Strategy Impact on Structural Assessment of Deteriorated Concrete Bridge Columns. *Proceedings of the Institution of Civil Engineers-Bridge Engineering* 175 (4): 246–262. https://doi.org/10.1680/jbren.21.00003.

Afsar Dizaj, E. & Kashani, M.M. 2022. Nonlinear Structural Performance and Seismic Fragility of Corroded Reinforced Concrete Structures: Modelling Guidelines. *European Journal of Environmental and Civil Engineering* 26(11): 5374–5403. https://doi.org/10.1080/19648189.2021.1896582.

Afsar Dizaj, E. & Kashani, M.M. 2022. Influence of ground motion type on nonlinear seismic behaviour and fragility of corrosion-damaged reinforced concrete bridge piers. *Bulletin of Earthquake Engineering* 20: 1489–1518. https://doi.org/10.1007/s10518-021-01297-5.

Afsar Dizaj E, Padgett J.E., Kashani, M.M. 2021. A Markov Chain-Based Model for Structural Vulnerability Assessment of Corrosion-Damaged Reinforced Concrete Bridges. *Philosophical Transactions of The Royal Society A Mathematical Physical and Engineering Sciences* 379 (2203). https://doi.org/10.1098/rsta.2020.0290.

Afsar Dizaj, E., Salami, M.R., Kashani, M.M. 2022. Nonlinear dynamic behaviour and seismic fragility analysis of irregular multi-span RC bridges. *Structures* 44: 1730–1750. https://doi.org/10.1016/j.istruc.2022.08.112.

Afsar Dizaj, E., Salami, M.R., Kashani, M.M. 2023. Seismic vulnerability analysis of irregular multi-span concrete bridges with different corrosion damage scenarios. *Soil Dynamics and Earthquake Engineering* 107678. https://doi.org/10.1016/j.soildyn.2022.107678.

American Society of Civil Engineers. 2021. Report card for America's infrastructure. http://www.infrastructurereportcard.org.

Broomfield, J.P. 2007. Corrosion of Steel in Concrete, Understanding, investigation and repair. Taylor & Francis, London.

Caltrans. 2013. Caltrans Seismic Design Criteria-Version 1.7. Sacramento, California: California Department of Transportation.

Camacho, V.T., Lopes, M., Oliveira, C.S. 2022. Multivariate analysis of regular and irregular RC bridges and characterization of earthquake behaviour according to stiffness-based indexes. *Bulletin of Earthquake Engineering*, 20: 415–448. https://doi.org/10.1007/s10518-021-01223-9.

Choe, D.E., Gardoni, P., Rosowsky, D., Haukaas, T. 2009. Seismic fragility estimates for reinforced concrete bridges subject to corrosion. *Structural Safety* 31(4): 275–83. https://doi.org/10.1016/j.strusafe.2008.10.001.

Comptroller and Auditor General, Maintaining Strategic Infrastructure: Roads, HC 169, Department for Transport and Highways Agency, London, 6 June 2014.

FEMA P695. 2009. Quantification of building seismic performance factors. Federal Emergency Management Agency, Washington, DC.

Ghosh, J., & Sood, P. 2016. Consideration of time-evolving capacity distributions and improved degradation models for seismic fragility assessment of aging highway bridges. *Reliability Engineering & System Safety* 154: 197–218. https://doi.org/10.1016/j.ress.2016.06.001.

Gómez-Soberón, M.C., Pérezm E., Salas, D., León-Escobedo, D.D. 2019. Seismic vulnerability through drift assessment for bridges with geometrical irregularities. *European Journal of Environmental and Civil Engineering*. https://doi.org/10.1080/19648189.2019.1686428.

Guirguis, JEB., Mehanny, SSF. 2012. Evaluating code criteria for regular seismic behavior of continuous concrete box girder bridges with unequal height piers. *Journal of Bridge Engineering* 18(6):486–498. DOI: 10.1061/(ASCE)BE.1943-5592.0000383.

Hu, Y. & Guo W. 2020. Seismic response of high-speed railway bridge-track system considering unequal-height pier configurations. *Soil Dynamics and Earthquake Engineering* 137: 106250. https://doi.org/10.1016/j.soildyn.2020.106250.

Ishac, MG., Mehanny, SSF. 2017. Do mixed pier-to-deck connections alleviate irregularity of seismic response of bridges with unequal height piers? *Bulletin of Earthquake Engineering*, 15(1): 97–121. https://doi.org/10.1007/s10518-016-9958-8.

Jara, J.M., Villanueva, D., Jara, M., Olmos, B.A. 2013. Isolation parameters for improving the seismic performance of irregular bridges. *Bulletin of Earthquake Engineering*, 11: 663–686. https://doi.org/10.1007/s10518-012-9398-z.

Jara, J.M., Reynoso, J.R., Olmos, B.A., Jara, M. 2015. Expected seismic performance of irregular medium-span simply supported bridges on soft and hard soils. *Engineering Structures* 98:174–185. https://doi.org/10.1016/j.engstruct.2015.04.032.

Johnson, N., Ranf, RT., Saiidi, M.S., Sanders, D., and Eberhard, M. 2008. Seismic testing of a two-span reinforced concrete bridge. *Journal of Bridge Engineering* 13(2): 173–182. https://doi.org/10.1061/(ASCE)1084-0702(2008)13:2(173).

Kappos, AJ., Manolis, GD., Moschonas, IF. 2002. Seismic assessment and design of R/C bridges with irregular configuration, including SSI effects. *Engineering Structures* 24(10): 1337–1348. https://doi.org/10.1016/S0141-0296(02)00068-8.

Priestley, M. J. N. 2007. The need for displacement-based design and analysis. Advanced earthquake engineering analysis, Vol. 494, *CISM International Center for Mechanical Sciences*, Springer, Vienna, Austria, 121–132.

Saiidi, M.S., Vosooghi, A., Nelson, R.B. 2012. Shake-table studies of a four-span reinforced concrete bridge. *Journal of Structural Engineering* 139(8): 1352–1361. https://doi.org/10.1061/(ASCE)ST.1943-541X.0000790.

Salami M.R, Afsar Dizaj E, Kashani M.M. 2019. The behavior of Rectangular and Circular Reinforced Concrete Columns under Biaxial Multiple Excitation. *ComSputer Modeling in Engineering & Sciences* 120 (3): 677–691. https://doi.org/10.32604/cmes.2019.05666.

Soleimani, F., Vidakovic, B., DesRoches, R., Padgett, J. 2017. Identification of the significant uncertain parameters in the seismic response of irregular bridges. Engineering Structures 141: 356–372. http://dx.doi.org/10.1016/j.engstruct.2017.03.017.

Soltanieh, S., Memarpour, M.M., Kilanehei, F. 2019. Performance assessment of bridge-soil-foundation system with irregular configuration considering ground motion directionality effects. *Soil Dynamics and Earthquake Engineering* 118: 19–34. https://doi.org/10.1016/j.soildyn.2018.11.006.

Xiang N. & Li J. 2020. Utilizing yielding steel dampers to mitigate transverse seismic irregularity of a multi-span continuous bridge with unequal height piers. *Engineering Structures* 110056, https://doi.org/10.1016/j.engstruct.2019.110056.

Zhang, Y., DesRoches, R., Tien, I. 2019. Impact of corrosion on risk assessment of shear-critical and short lap-spliced bridges. *Engineering Structures*, 189: 260–271. https://doi.org/10.1016/j.engstruct.2019.03.050.